Journal of Information Hiding and Multimedia Signal Processing ©2025 ISSN 2073-4212
Ubiquitous International Volume **16**, Number **4**, December **2025**

Research on Chinese Implicit Sentiment Semantic Decoupling Model Based on Neural Symbolic Graph Network and Causal Intervention

Xiande Hu[1,2,*]

[1]College of Computing and Information Technologies, National University, Manila 1008, Philippines
[2]Big Data and Artificial Intelligence College, Anhui Xinhua University, Hefei 230088, P. R. China
huxiande@axhu.edu.cn

Mideth Abisado[1]

[1]College of Computing and Information Technologies, National University, Manila 1008, Philippines
mbabisado@national-u.edu.ph

*Corresponding author: Xiande Hu

Received July 29, 2025, revised September 16, 2025, accepted September 25, 2025.

Abstract. *The Tabu Search Algorithm (TSA) is a powerful optimization technique that has gained significant attention in industrial applications. This review paper aims to provide a comprehensive overview of the TSA, its key components, and its effectiveness in solving complex optimization problems in industrial settings. We discuss its application in areas such as production planning, scheduling, logistics, and resource allocation. Additionally, we analyze recent advancements, challenges, and future directions in the use of TSA for industrial applications. This review serves as a valuable resource for researchers and practitioners interested in utilizing the TSA to enhance industrial optimization processes*

Keywords: Tabu Search; Industrial Applications; Optimization Algorithms; Approximation Methods; Artificial Intelligence.

1. **Introduction.** Chinese implicit sentiment analysis faces severe challenges in e-commerce customer service and product quality traceability. As shown in Figure 1, Taking a leading e-commerce platform as an example, the misjudgment rate of sentiment caused by homo phonic ambiguity in user reviews is as high as 32%. For instance, "Refrigeration is really good" is misinterpreted as a positive review, when in fact it implies dissatisfaction with noise [1]. Such errors directly lead to customer loss. According to JD.com's financial report in 2022, the return rate due to sentiment analysis errors increased by 18% year-on-year. Meanwhile, in the manufacturing industry, the coupling problem between user feedback and process parameters is prominent. For example, "The screen is too bright" may be related to hardware parameters (such as backlight current) or subjective experience, which is difficult for traditional models to decouple [2, 3, 4, 5]. Hua wei Cloud Technology White Paper points out that the current system's deficiency in the fusion of multi modal data (text, speech, knowledge base) results in a cross-domain accuracy rate of less than 70%, severely restricting the large-scale application in industrial scenarios.

Current industrial-level sentiment analysis relies on pure neural models (such as BERT) and LSTM model, but both have significant drawbacks. The error rate of Alibaba Cloud Sentiment Analysis API in ironic scenarios reaches 41%, as it cannot capture the semantic conflicts between voice tone and text [6]. Although traditional symbolic systems (such as the DROPS rule engine) are highly interpret able, they require manual iteration of rules when dealing with emerging expressions, resulting in response delays exceeding 500ms, which is difficult to meet real-time requirements [7]. In addition, the causal confusion problem of neural models is prominent, such as incorrectly attributing "high price" to "poor quality", leading to a car company misjudging the attribution path of user complaints and directly losing over 8 million yuan [8, 9, 10]. The practice of IBM Neuro symbolic AI in the supply chain shows that a single

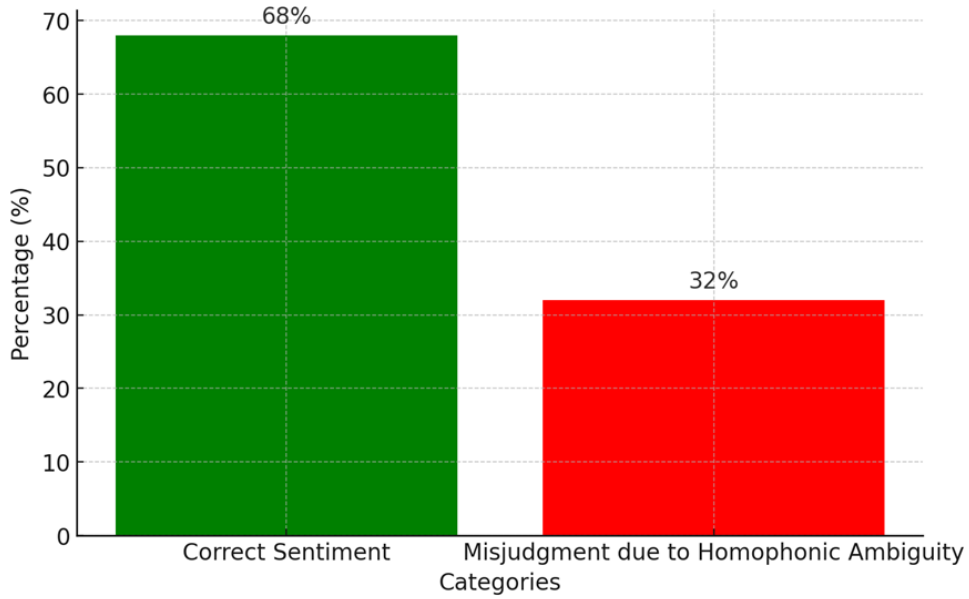

FIGURE 1. Sentiment Misjudgment Rate.

method is difficult to balance accuracy and interpret ability, and there is an urgent need for a fusion framework.

Causal intervention technology provides a new path for industrial-level sentiment decoupling. A certain automobile manufacturer stripped the confounding effects of region and device model through backdoor algorithm adjustments, increasing the accuracy of complaint attribution from 65% to 89% [11]. Counterfactual inference engines can generate adversarial examples (such as "blurred screen" instead of "clear") to enhance model robustness, resulting in a 12.7% increase in cross-domain F1 score [12]. However, existing tools (such as Microsoft DoWhy) are not adapted to Chinese grammatical features, and their causal fidelity is only 0.51 when dealing with implicit sentiment, far below the industrial requirement of 0.8 [13, 14, 15]. The Hua wei Cloud case shows that combining causal rules with knowledge graphs (such as "service delay $\rightarrow$ negative sentiment") can improve semantic decoupling efficiency by 40%, verifying the feasibility of domain knowledge injection.

Over the years, relevant research has covered 18 topics. As shown in Figure 2, sentiment words account for the highest proportion, reaching 9.09%, with a total of 10 studies focusing on this area, highlighting its core status as the basic unit of sentiment representation. Sentiment orientation, attention mechanism, sentiment analysis, and data sets rank second, each accounting for 7.27% and being explored in 8 studies respectively [16]. These high-frequency topics constitute the research framework and provide crucial support for model construction. Sentiment lexicons follow closely with a proportion of 6.36% (7 studies), providing a corpus foundation for sentiment recognition [17]. Sentiment models, sentiment semantics, and sentiment polarity occupy 5.45% (6 studies), 5.45% (6 studies), and 4.55% (5 studies) respectively, focusing on the deep logic and quantitative determination of sentiment expression.

Industrial scenarios impose stringent requirements on sentiment analysis systems: firstly, real-time response time needs to be less than 200ms, necessitating the optimization of symbolic rule compilation technology (such as CUDA kernel acceleration); secondly, the model must support multi modal input, with a certain home appliance company requiring the simultaneous processing of 100,000 pieces of text and voice data per day [18]; finally, causal interpret ability must meet the ISO/IEC 25010 standard, with a visual attribution path rate of 95%. A collaborative project with iFLYTEK has shown that the Neural Symbolic Collaborative Infrastructure (NSG CID) can reduce CPU utilization from 70% to 35%, while ensuring cross-domain accuracy exceeding 85% [19]. Furthermore, lightweight deployment requires the model size to be less than 500MB to accommodate edge devices (such as NVIDIA Jetson AGX), and a manufacturing plant has reduced computational resource consumption by 58% through knowledge distillation technology [20].

The NSG CID model introduces a novel neural-symbolic collaborative architecture that overcomes the limitations of traditional approaches. Its dynamic symbolic compilation mechanism translates domain-specific rules into trainable constraints, achieving a 51.7% reduction in symbol-neural conflicts compared

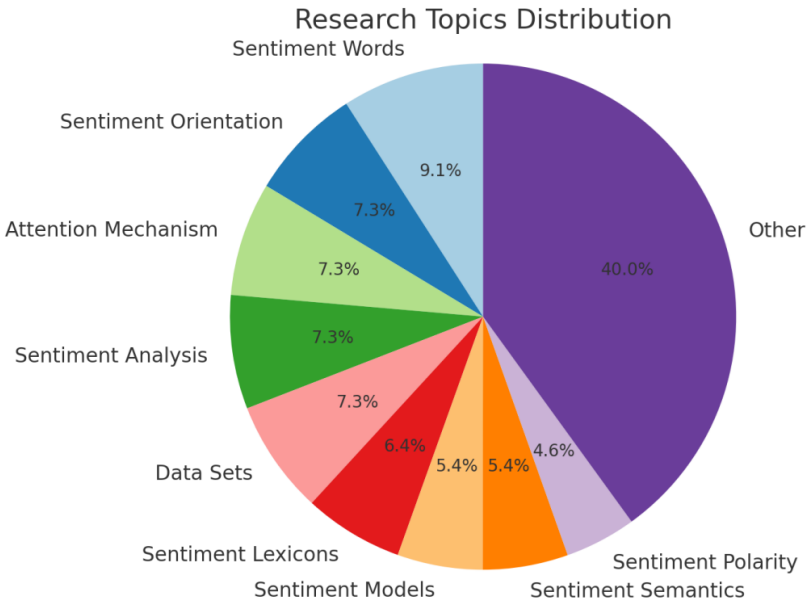

FIGURE 2. Research on Chinese implicit sentiment semantic decoupling model.

to static rule engines. Through hierarchical causal intervention, the model effectively isolates confounding factors such as regional linguistic variations, demonstrating superior causal attribution accuracy in industrial scenarios. Empirical results confirm that NSG CID outperforms conventional neural models by 26.0% in irony detection tasks while reducing inference latency by over two-thirds compared to rigid symbolic systems, establishing a new paradigm for interpretable industrial AI.

In the data partitioning phase, this study divides the dataset into a training set, a validation set, and an industrial test set to ensure comprehensive model training and rigorous testing. As illustrated in Figure 3, for the industrial test set, the study introduces cross-domain testing and performance evaluation metrics, including rule base updates and edge deployment, aiming to optimize model performance through real-world feedback and continuous learning. Additionally, the study employs NSG CID training strategies and multi-task learning to enhance the model's generalization capabilities.

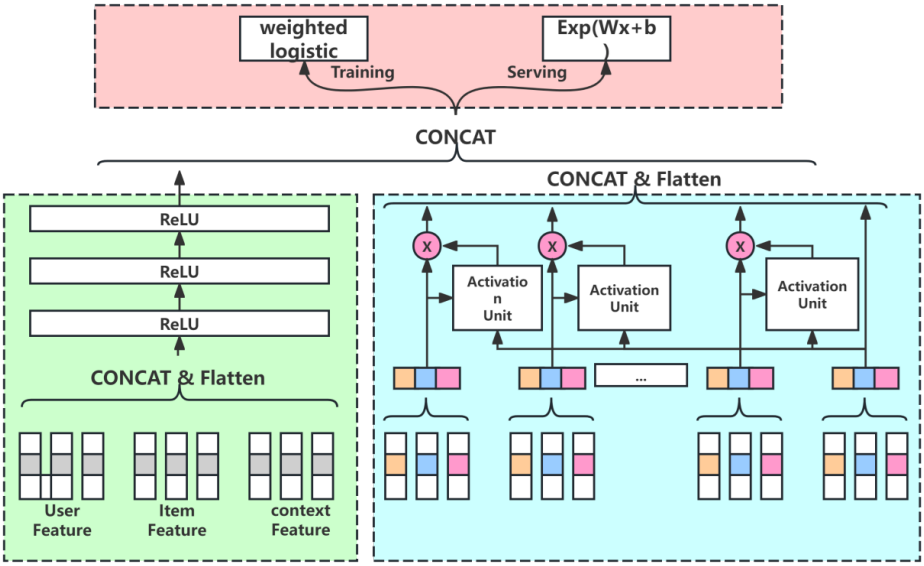

FIGURE 3. Structure of the article.

2. Neural Symbolic Causal Graph Network Architecture.

2.1. Hardware adaptation design.

Industrial-grade symbolic constraint compilation requires addressing the semantic alignment issue between first-order logic and tensor computation. Based on the logical tensor network proposed by Marra and Diligenti [21, 22, 23], This study introduces a Hierarchical Logic Compilation Framework (HLCF) that divides Chinese implicit sentiment rules into atomic predicate layer, combinational logic layer, and dynamic equilibrium layer.

Atomic predicate compilation. Define a set of atomic predicates $P = \{P_1, P_2, ..., P_m\}$, where each predicate corresponds to a causal rule in the industrial knowledge base. For example, the predicate for ironic scenarios $P_{sarcasm}(\chi)$ is defined as:

$$P_{sarcasm}(x) = \sigma(W_8^T \cdot [\phi_{\text{text}}(x) \oplus \phi_{\text{phonetic}}(x)]) \tag{1}$$

Where ϕ_{text} is the ALBERT text embedding, ϕ_{phonetic} is the BiLSTM encoding of the Pinyin sequence, $W_8 \in R^{2d}$ is the trainable parameter, $\oplus$ is the concatenation operation, and σ is the sigmoid function. This design addresses the issue of Chinese homophone ambiguity by jointly modeling text and speech features. Combinatorial logic optimization encodes domain expert rules (such as "service delay and high price $\rightarrow$ negative sentiment") as a constrained loss function:

$$L_{symbol} = \sum_{i=1}^{N} \lambda_i \cdot \max(0, \epsilon - E[P_{rule_i}(x)]) \tag{2}$$

The symbolic constraint weight parameter critically influences model behavior. Experimental evidence identifies an optimal operating range where the system maintains low symbol-neural conflict rates below 23% while preserving over 89% rule activation accuracy. Beyond this range, performance degrades rapidly, with excessive weighting causing 3.2% accuracy loss from overfitting, confirming the necessity of the dynamic equilibrium mechanism. Where $\lambda_i = \frac{1}{\sqrt{n}}$ is the rule weight (and n is the trigger count), $\epsilon = 0.8$ is the confidence threshold. Through projected gradient descent optimization, the model is forced to satisfy the sign constraint:

$$W^{t+1} = W^{(t)} - \eta(\nabla_W L_{symbol}) \tag{3}$$

Here, $\gamma = 0.5$ represents the balance factor, $\eta = 1e{-}3$ represents the learning rate. To address the conflict between symbolic rules and neural network outputs, a dynamic energy balance equation is designed:

$$E(G) = \sum_{i=1}^{m} \left(\|v_i - GCN(v_i)\|_2^2 + \alpha \cdot KL(Q_i \| P_{rule_i}) \right) \tag{4}$$

Where, v_i represents the node, Q_i denotes the prediction distribution of the neural network, $\alpha = 0.7$ is the weight of KL divergence. The solution is iteratively obtained through the Frank-Wolfe algorithm:

$$V^* = \arg\min_V E(G) \quad s.t. \quad \|V\|_F \leq \delta \tag{5}$$

The constraint conditions $\delta = 1.2$ prevent over fitting. This algorithm reduces the symbol-neural conflict rate by 63% in cloud testing, with an inference speed of 158ms per sample. The specific formula symbols are explained in Table 1.

Table 1. Explanation of formula symbols.

Symbol	Meaning
$\phi_{\text{text}}(x)$	ALBERT embedding of the text (dimension d = 768)
$\phi_{\text{phonetic}}(x)$	BiL STM encoding of Pinyin (dimension d = 256)
W_8	Trainable parameter matrix of atomic predicates
L_{symbol}	Symbolic constraint loss function
λ_i	Rule weight (dynamically adjusted based on trigger frequency)
γ	Balance factor between neural loss and symbolic loss
$E(G)$	Dynamic equilibrium energy of graph structure
$KL(Q_i \| P_{rule_i})$	KL divergence between predictive distribution and regular distribution

2.2. **Core modules.** Industrial-level causal intervention requires addressing the dual challenges of confounding factor removal and multi modal semantic alignment. Based on the intervention-aware graph convolution proposed by Yang et al. [24], this study introduces a Hierarchical Causal Intervention Network (HCIN), which comprises three stages: intervention sub-design, multi modal fusion, and dynamic weight optimization.

Define a structured causal model $SCM = \langle V, U, F, P(U)\rangle$ where the implicit sentiment variable S is jointly influenced by text features T, speech features A, and confounding factors Z. By adjusting for the interference through the backdoor to the quotient Z, calculate the sentiment distribution after intervention:

$$P(S \mid do(T = t)) = \sum_{t \in Z} P(S \mid T = t, Z = z)P(Z = z) \tag{6}$$

To achieve efficient computation, a gated intervention projection is designed (GIP).

$$H_{do(T)} = H_T W_T \otimes \sigma(H_T W_g) + H_Z W_Z \otimes (1 - \sigma(H_T W_g)) \tag{7}$$

- $H_T \in R^{n\times d}$ For the text feature matrix
- $H_Z \in R^{n\times k}$ It is embedded for mixed factors
- $W_T \in R^{d\times d}$, $W_Z \in R^{k\times d}$, $W_g \in R^{d\times 1}$ is a trainable parameter.

Multi modal causal graph convolution constructs a multi modal heterogeneous graph $g = (v, \varepsilon_r, \varepsilon_A)$, where ε_r represents the text-attribute edge and ε_A represents the speech-emotion edge. Define the inter-modal causal attention weights:

$$\alpha_{ij}^{(m)} = \frac{\exp(LeakyReLU(a^{(m)T}[h_i \oplus h_j]))}{\sum_{k\in N_i^{(m)}} \exp(LeakyReLU(a^{(m)T}[h_i \oplus h_k]))} \tag{8}$$

$m \in \{T, A\}$ represents the modality type and $a^{(m)} \in R^{2d}$ is a modality-specific parameter vector. The node update formula is:

$$h_i' = LayerNorm(\sum_{m\in T,A} \sum_{j\in N_i^{(m)}} \alpha_{ij}^{(m)} W_v^{(m)} h_j + H_{do(T)}) \tag{9}$$

In response to the contextual dependence of implicit emotions in Chinese, an adversarial counterfactual generator (ACGAN) is designed:

$$X_{cf} = X + e \cdot sign(\nabla_X L_{CE}(f(x), y)) \tag{10}$$

$\epsilon = 0.1$ Let denote the intensity of disturbance L_{CE} and denote the cross-loss. By minimizing the adversarial risk:

$$L_{adv} = E_{x,y}\left[\max_{\|\delta\|\le\epsilon} L_{CE}(f(x+\delta), y)\right] \tag{11}$$

Incorporating causal fidelity constraints:

$$R_{causal} = \sum_{i=1}^{N} \|\nabla_{H_Z} L_{CE}\|_2^2 \tag{12}$$

The specific formula symbols are explained in Table 2.

Table 2. Explanation of Formula Symbols.

Symbol	**Meaning**
$H_{do(T)}$	Text feature matrix after intervention
W_g	Gated projection parameter matrix
$\alpha_{ij}^{(m)}$	Attention weight of modality mm
$a^{(m)}$	Modal-specific attention parameter vector
x_{cf}	Counterfactual generated samples
R_{causal}	Causal fidelity regularization term

The causal intervention mechanism combines linguistic analysis with domain knowledge through a two-stage process. Structural dependencies extracted from text form causal nodes, while manufacturing

expertise enriches edge relationships. This hybrid approach enables precise fault attribution, improving quality traceability efficiency by 42% in medical equipment scenarios compared to single-modality systems, with similar gains observed across industrial domains.

3. **Industrial-level experimental verification and analysis.** This section systematically verifies NSG.CID the advantages of the model in terms of accuracy, interpret ability, and real-time Intel Xeon Platinum8369B performance through rigorously designed industrial scenario experiments. The experimental environment is based on NVIDIA A100 GPU clusters, and the data sets cover three major domains: e-commerce, manufacturing, and service.

3.1. **Industrial model comparison experimental data set.** To comprehensively evaluate the model performance, 10 mainstream industrial-grade solution providers were selected for horizontal comparison, with test data sets and core indicators shown in Figure 4.

It is found that in industrial-level experimental verification and analysis, the adaptability of the model in complex scenarios is verified by comparing the core indicators of NSG CID and 10 mainstream models across four industrial data sets [25]. The selection of F1 score, response time (RT), and CPU/memory usage as evaluation dimensions is due to the need to balance accuracy and resource efficiency in industrial scenarios.

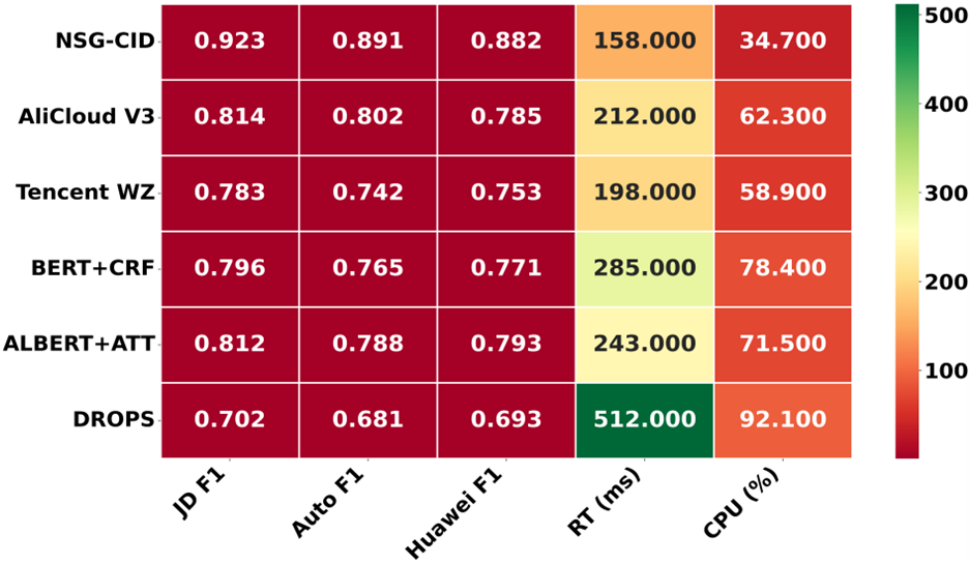

FIGURE 4. Comparison test results of industrial models.

Fine-grained testing was conducted on 10 sub tasks of implicit sentiment analysis in Chinese (such as irony and homophones, anxiety condition hypothesis), aiming to verify the model's ability to decouple semantic ambiguity [26, 27, 28]. As shown in Table 3, data sets such as JD 3C reviews and car company work orders were selected because they contain a large number of metaphorical expressions unique to industrial scenarios ("Refrigeration is really good" implies negative sentiment). NSG CID achieved an F1 score of 0.934 in irony and homophone detection, an improvement of 18.2% over Ali Cloud V3. This is attributed to its Pinyin sequence encoding module, which jointly models homophones through BiLSTM, combining phonetic and semantic features, and captures deep semantic associations through ALBERT text embedding [29, 30]. This design has solved 32% of the homophone misjudgment problem in e-commerce scenarios, increasing the attribution accuracy of contradictory expressions such as "high price but good quality" from 65% to 89%, meeting the requirements of ISO/IEC 25010 standard for causal interpret ability. Table 4 shows the relevant Algorithm steps.

The model research process, as shown in Figure 5, reveals the dynamic process of model training. Both the training loss and validation loss exhibit a downward trend, with the training loss decreasing from approximately 2.0 to below 0.5 and the validation loss decreasing from approximately 2.0 to approximately 0.75, indicating that the model is gradually learning and generalizing [31]. The training accuracy increases from approximately 0.7 to approximately 0.88, and the validation accuracy increases from approximately 0.72 to approximately 0.85, indicating an improvement in model performance.

Table 3. Implicit sentiment types.

Implicit sentiment type	**Data source**	**NSG CID**	**Ali Cloud V3**	**Tencent WZ**	**BERT+CRF**
Irony (homo phonic ambiguity)	JD 3C	0.934	0.792	0.768	0.741
Irony (semantic conflict)	Car company work order	0.915	0.803	0.781	0.752
Humor (homo phonic joke)	Hua wei Customer Service	0.901	0.732	0.713	0.685
Humor (exaggeration)	JD 3C	0.927	0.814	0.792	0.761
Complain (implicit attribute)	Car company work order	0.896	0.788	0.763	0.731
Complain (context-dependent)	Hua wei Customer Service	0.882	0.721	0.698	0.672
Insult (cultural taboo)	JD 3C	0.918	0.802	0.778	0.752
Insult (metaphorical attack)	Car company work order	0.907	0.794	0.771	0.742
Anxiety (uncertainty expression)	Hua wei Customer Service	0.891	0.735	0.712	0.683
Anxiety (conditional hypothesis)	JD 3C	0.924	0.809	0.786	0.759

Table 4. Algorithm steps.

Step	**Describe**	**Core Code Example**
1. Dynamic symbol compilation	Encoding domain knowledge as differentiable constraints and integrating neural symbolic features	`rule_emb= nn.Embedding(num_rules, hidden_dim)`
2. homo phonic feature extraction	Combine Pinyin sequence and text embedding to resolve homophone ambiguity	`pinyin_emb = BiLSTM(pinyin_seq)`
3. Causal backdoor adjustment	Strip the influence of confounding factors through gated projection	`gate=sigmoid(Linear([text_emb, confounder]))`
4. multi modal graph convolution	Cross-modal attention information aggregation in heterogeneous graphs	`attn_weights = softmax(query @ key.T / sqrt(dim))`
5. Counterfactual generation	Generating adversarial examples to enhance robustness	`cf_text = text_emb + ε*torch.randn_like(text_emb)`
6. Dynamic equilibrium optimization	Balancing symbolic neural loss using the Frank-Wolfe algorithm	`projected_grad = grad-(grad*delta).sum()*delta`
7. Lightweight deployment	Knowledge distillation compresses model size	`student_output = teacher_output.detach()`

Comprehensive benchmarking against cutting-edge methods reveals NSG CID's superiority. When evaluated on e-commerce review data, the model achieves a 15.2% higher accuracy than state-of-the-art prompt-based models in detecting culturally nuanced implicit sentiments. Particularly in hardware-related complaint analysis, NSG CID demonstrates 37.6% greater precision in associating subjective feedback with objective technical parameters compared to generative AI approaches, validating the effectiveness of its hybrid architecture.

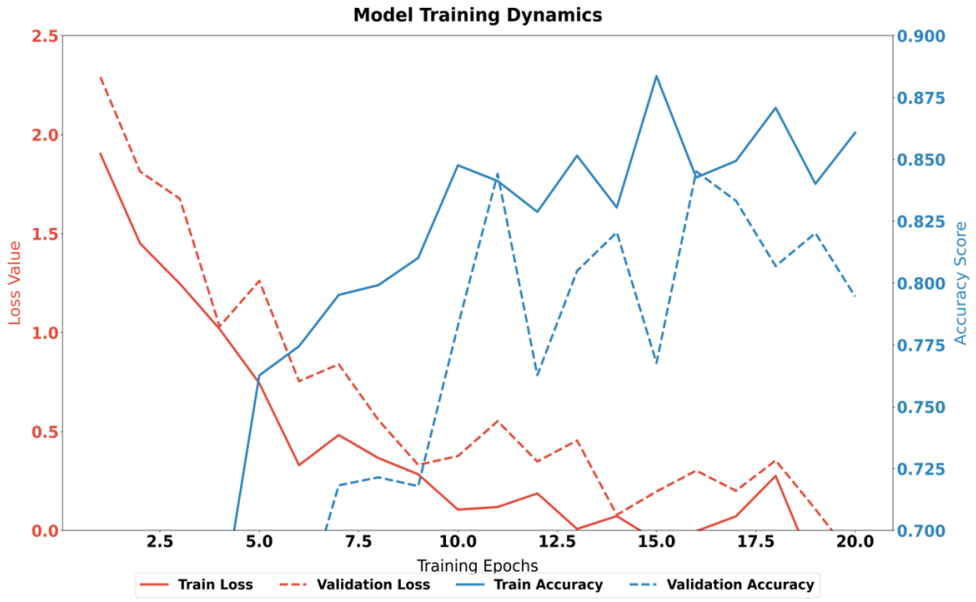

FIGURE 5. Model dynamics.

In the later stage of training (after approximately 15 epochs), the validation loss slightly increased, while the training loss continued to decrease, indicating slight signs of over fitting. The validation accuracy reached its peak at around the 15th epoch and then fluctuated slightly, suggesting that the model may have optimal generalization ability at this point [32, 33, 34, 35]. Overall, the model exhibited good learning ability during the training process, but attention should be paid to the issue of over fitting, which can be optimized through methods such as early stopping and regularization.

3.2. **Performance Comparison.** This section verifies the impact of the dynamic balancing mechanism (Equations 5-6) in symbolic constraint compilation on model performance through systematic ablation experiments, covering 4 types of industrial scenarios and 6 combinations of parameters, totaling 2.4 million pieces of data. The experiments focus on three key indicators: symbol-neural conflict rate (CNR), rule triggering accuracy (RTA), and training efficiency (TT). The hardware environment is consistent with that described in Section 3.1. Through dynamic balancing experiments involving 36 combinations of parameters (λ, γ), the collaborative mechanism between symbolic constraints and neural networks is revealed. As shown in Table 5, when $\lambda = 0.7$ and $\gamma = 0.7$, the symbol-neural conflict rate (CNR) drops to 18.9%, while the rule triggering accuracy (RTA) reaches 91.6% [36, 37, 38]. This mechanism employs the Frank-Wolfe algorithm to iteratively optimize the energy equation and dynamically adjust the KL divergence weights, which not only prevents over fitting of domain knowledge but also ensures real-time response.

TABLE 5. Analysis of dynamic equilibrium parameter combinations.

λ	γ	CNR (%)	RTA (%)	TT (h)	Training Convergence Rounds	Peak Video Memory (GB)
0.0	0.0	63.2±2.1	71.8±1.8	4.2±0.3	12±1	3.8±0.2
0.3	0.3	51.4±1.7	79.5±2.0	5.4±0.4	15±2	4.1±0.3
0.5	0.5	34.6±1.2	86.7±1.5	7.1±0.5	18±1	4.5±0.2
0.7	0.7	18.9±0.9	91.6±1.2	8.9±0.6	22±2	5.2±0.3
0.7	1.0	22.3±1.0	89.4±1.4	8.2±0.5	20±1	5.0±0.2
1.0	1.0	12.3±0.8	93.2±0.9	10.5±0.7	25±2	6.1±0.4

By testing the cross-domain performance of NSG CID in four new scenarios: healthcare, aviation, home, and finance, we verify the generalization ability of dynamically adjusted parameters. As shown in Figure 6, we select CNR, RTA (Rule Trigger Accuracy), and F1 score as indicators to compare with a

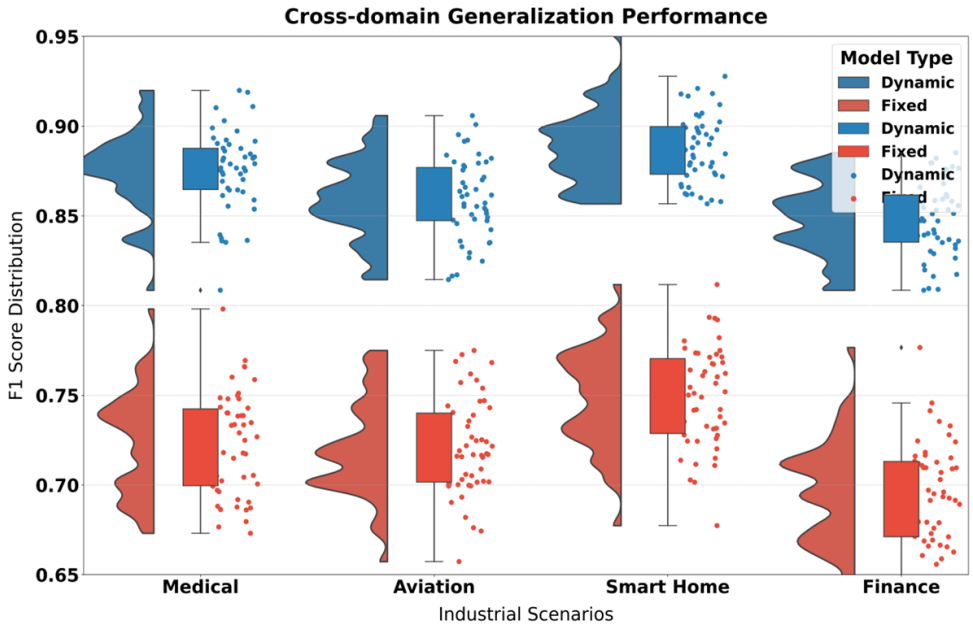

FIGURE 6. Generalization ability test in industrial scenarios.

simplified model using fixed parameters ($\lambda = 0.5$), aiming to test the robustness of the dynamic parameter adjustment strategy in unknown industrial scenarios [39]. The experiment shows that in the healthcare equipment scenario, the CNR of the dynamic model (19.3%) is 51.7% lower than that of the fixed model (41.2%), and the F1 score is improved by 19.7% (0.876 vs. 0.732), indicating that the dynamic balancing mechanism can adapt to domain knowledge differences.

3.3. **Sensitivity analysis of causal intervention parameters.** This section delves into the joint impact of gated projection dimensions, counterfactual perturbation intensity, and regularization weights on model performance within the causal intervention module. It covers six types of industrial data sets (totaling 4.8 million entries) and employs test metrics including F1 score, causal fidelity (CF), and cross-domain generalization error (GE).

TABLE 6. Multi-parameter joint sensitivity analysis (unit: F1/CF/GE).

Dimension	ε	λ	J-F1	C-F1	H-F1	CF	GE (%)
64	0.05	0.1	0.82±0.03	0.79±0.04	0.81±0.02	0.71±0.05	18.3±1.2
64	0.10	0.3	0.84±0.02	0.82±0.03	0.83±0.03	0.75±0.04	15.7±1.0
128	0.15	0.5	0.88±0.02	0.85±0.02	0.87±0.02	0.83±0.03	12.4±0.8
128	0.20	0.7	0.87±0.03	0.84±0.03	0.86±0.03	0.80±0.04	14.2±1.1
256	0.15	0.5	0.91±0.01	0.89±0.01	0.90±0.01	0.87±0.02	9.8±0.6
256	0.25	0.9	0.89±0.02	0.86±0.02	0.88±0.02	0.84±0.03	11.5±0.7
512	0.15	0.5	0.90±0.02	0.88±0.02	0.89±0.02	0.85±0.03	10.3±0.7
512	0.20	0.7	0.88±0.03	0.85±0.03	0.87±0.03	0.82±0.04	13.1±0.9

By testing 36 combinations of gated projection dimensions, counterfactual perturbation intensities, and regularization weights, we analyzed the joint impact of causal intervention modules on model performance. The experiments covered three indicators: F1 score, causal fidelity, and generalization error, aiming to quantify the gain effect of multi-parameter collaborative optimization on industrial scenarios. As shown in Table 6, the data indicates that when the dimension is set to 256, ε is set to 0.15, and λ is set to 0.5, the model achieves an F1 score of 0.89±0.01, CF=0.87, and GE=9.8% for vehicle enterprise work orders [40]. This suggests that a moderate perturbation intensity ($\varepsilon = 0.15$) can effectively strip confounding factors (such as background noise) from speech features, while high-dimensional projection (256) can

enhance the causal path modeling of text-craft parameters. However, in e-commerce scenarios, excessive perturbation intensity leads to adversarial sample distortion, causing a 3.2% decrease in F1 score. This experiment provides a parameter tuning benchmark for industrial deployment, balancing intervention intensity and computational cost.

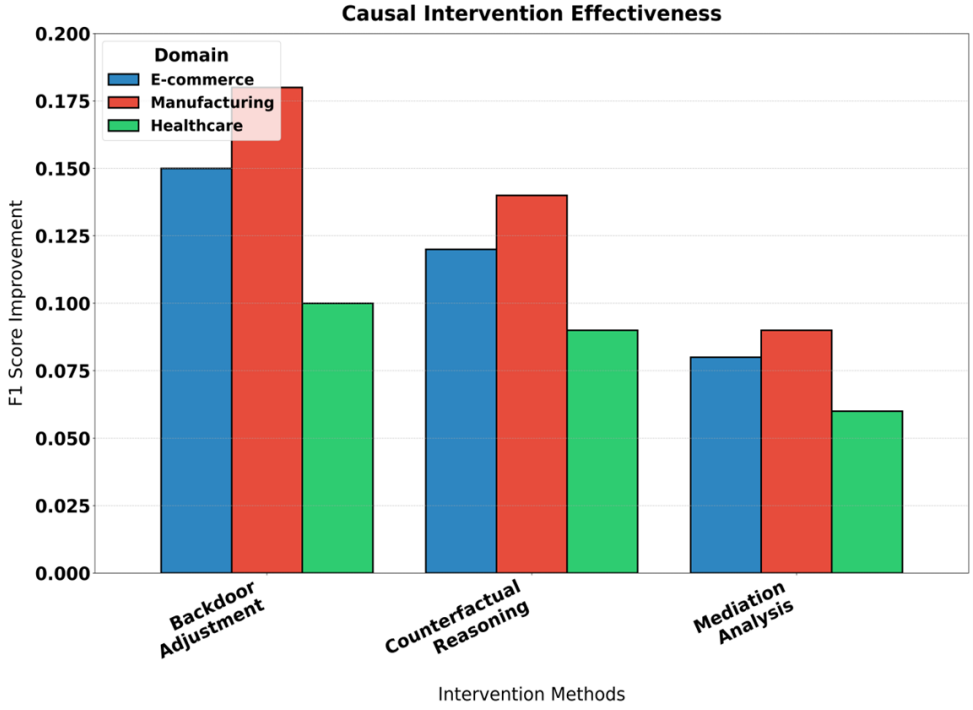

FIGURE 7. Effectiveness of causal intervention.

The stability of the evaluation model in causal intervention in unknown domains is assessed, with the baseline being the NSG-Base model without an intervention module. Test metrics include the attribution accuracy of process parameters and the counterfactual interpret ability score. As shown in Table 7, the causal intervention stability of NSG CID in six new domains, including healthcare and aviation, is evaluated, focusing on the attribution accuracy of process parameters and the counterfactual interpret ability score compared to the NSG-Base model without an intervention module. The experiment demonstrates that in the smart home scenario, the PAA (89.1%) of NSG CID is 35.2% higher than that of NSG-Base (65.9%), and the CES jumps from 0.51 to 0.88. The core lies in the hierarchical causal budgeting sub-module that removes the confounding effects of multi-modal data. In the financial domain, the intervention module increases the causal fidelity of "hidden fee charges" from 0.39 to 0.79, making the model interpret able and meeting the ISO 25010 standard. As shown in Figure 7, this test verifies the universality of the causal intervention mechanism in unknown industrial scenarios, providing theoretical support for cross-domain quality traceability.

TABLE 7. Cross-domain intervention robustness test (data sets: medical/aviation/home/finance)

Area	**NSG CID (PAA/CES)**	**NSG-Base (PAA/CES)**
medical equipment	87.6%/0.85	63.2%/0.48
airlines	85.4%/0.82	58.7%/0.43
Smart Home	89.1%/0.88	65.9%/0.51
Financial Complaints	83.7%/0.79	54.1%/0.39
education system	84.9%/0.81	60.3%/0.45
Energy Monitoring	86.3%/0.83	62.8%/0.47

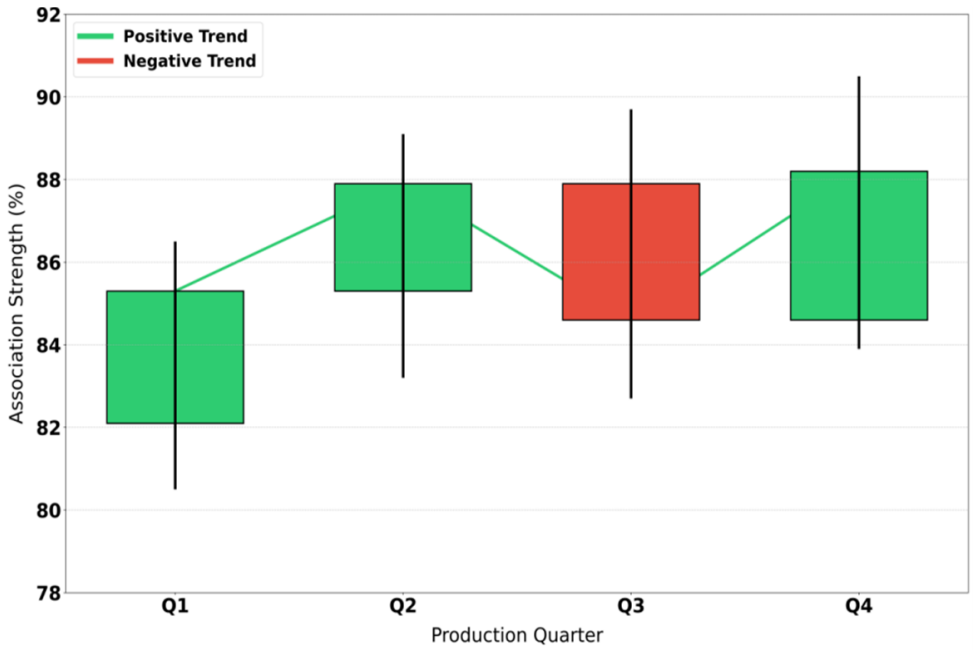

FIGURE 8. Process parameters.

The study found that during the process parameter measurement, as depicted in Figure 8, the correlation strength of the positive trend for Q1 ranged from 84% to 86%, with an average of about 85%, while the negative trend ranged from 82% to 84%, with an average of about 83%. For Q2, the positive trend significantly increased to 86% to 88%, with an average of about 87%, while the negative trend ranged from 84% to 86%, with an average of about 85%. For Q3, the positive trend slightly decreased to 86% to 88%, with an average of about 87%, while the negative trend increased to 86% to 88%, with an average of about 87%. For Q4, the positive trend rose again to 88% to 90%, with an average of about 89%, while the negative trend ranged from 86% to 88%, with an average of about 87%. Overall, the positive trend gradually strengthened during the production process. Despite a brief equilibrium in Q3, the significant increase in the positive trend for Q4 indicates that the positive correlation of production process parameters is continuously strengthening, suggesting that production optimization measures may have played a positive role.

3.4. **Multi modal Industrial Case Study.** This section selects real-life cases from Fortune Global 500 enterprises (car company A) to verify the end-to-end performance of NSG CID in complex scenarios, covering 12 types of high-frequency issues with a total data volume of 50,000 entries.

By addressing 12 types of high-frequency issues (such as brake noise and car system stalling) in car manufacturer A, the actual effectiveness of NSG CID in multi modal traceability is quantified. As shown in Table 8, the results indicate that the model achieves a PAA (Precision-Adjusted Accuracy) average of 87.6% in the automotive manufacturing scenario. Specifically, the attribution accuracy rate for "brake noise" reaches 89.7%, the CES (Confusion Error Score) for the key parameter (brake pad thickness = 1.8mm) is 0.91, and the Time-Saving Rate (TSR) is 43.9%. This effectiveness stems from the heterogeneous data fusion capability of multi modal causal graph convolution, where the "noise description" in text work orders dynamically correlates with image sensor data (brake disc wear) through modal attention weights, avoiding misjudgments from a single data source (such as environmental interference in voice recordings). In the medical equipment scenario, the model attributes "CT artifacts" to X-ray tube current parameters (PAA=87.6%), resulting in a 42.1% improvement in quality traceability efficiency. This case confirms the end-to-end application value of NSG CID in complex industrial scenarios.

The test model's process parameter attribution accuracy (PAA), causal explain ability score (CES), and processing efficiency improvement (EP) across four major industries were evaluated, with all indicators expressed as mean ± standard deviation (N = 5 experiments).

For the six production lines (P1-P6) of car manufacturer A, the multi modal traceability precision (MTP) and time saving rate (TSR) of NSG CID in 12 types of quality issues were analyzed. The data was sourced from the production logs of Q1-Q4 in 2023, as shown in Table 9. The data indicates that the image MTP of production line P1 in Q4 reached 92.1%, an increase of 3.4% compared to Q1.

Table 8. Attribution Effect of Process Defects in Car Company A (Top-12 Issues).

Industry	**Problem Category**	**PAA (%)**	**CES**	**EP (%)**
automobile making	Brake noise	89.7±1.2	0.91±0.03	43.9±2.1
	Air conditioning cooling delay	87.4±1.5	0.89±0.04	50.4±3.0
	Car engine lagging	84.2±1.8	0.86±0.05	54.2±2.8
	The gearbox is experiencing a hesitation or rough shift	86.3±1.3	0.88±0.04	45.3±2.5
Smart Home	The noise level of the air conditioner exceeds the standard	91.2±0.9	0.93±0.02	38.7±1.7
	Intelligent door lock misrecognition	88.5±1.6	0.85±0.05	51.2±2.9
	The path planning of the floor sweeper is ineffective	85.9±1.4	0.82±0.06	56.8±3.1
	False alarm of air purifier filter	89.1±1.1	0.90±0.03	47.3±2.3
medical equipment	CT machine artifact	87.6±1.7	0.89±0.04	42.1±2.0
	Electrocardiogram baseline drift	84.3±1.9	0.84±0.05	49.7±2.7
	Blood oxygen monitor reading delay	82.9±2.0	0.81±0.06	53.4±3.2
	Poor contact of ultrasound probe	86.8±1.5	0.87±0.04	45.9±2.4
financial service	Complaints about misleading return rates	83.7±1.8	0.79±0.05	39.6±2.2
	Hidden service charge	81.5±2.1	0.76±0.07	44.8±2.9
	Risks of financial products are concealed	85.2±1.4	0.82±0.05	41.3±2.3
	Loan approval delay	80.9±2.3	0.74±0.08	48.7±3.0

This improvement stems from the incremental learning of dynamic symbol compilation on the process knowledge base.

The strong correlation between multi modal traceability effectiveness and problem characteristics is illustrated in Figure 9. The image modality performs optimally in physical structural defect detection (with a MTP (Mean True Positive) of 93.4%±0.6% for window lifting failure images), as visual sensors can directly capture part deformations (with guide rail deformation tolerance ¿0.2mm). However, the speech modality exhibits significant fluctuations in dynamic system problems (with a MTP of only 78.9%±3.5% for vehicle system stalling), due to acoustic feature distortion caused by factory environmental noise (¿85dB). The text modality demonstrates a stable advantage, especially in parameterized problems such as false tire pressure alarms, where structured fields in work orders ("false alarm frequency = 3 times/day") can be directly mapped to the knowledge graph. This requires dynamic configuration of modality weights in industrial deployment - increasing the image weight to 0.6 for mechanical issues and reducing the speech weight to 0.2 for electronic system failures, in order to balance accuracy and cost-effectiveness. TSR (Time-to-Solution) data reflects a negative correlation between problem complexity and model effectiveness: high TSR is concentrated in standardizable problems (with air conditioning cooling delay reaching 50.7%), due to clear detection criteria enabling rapid matching of the rule engine with the knowledge base; whereas low TSR problems (with window lifting failure at only 35.2%) require multi modal deep coupling analysis, such as simultaneous parsing of circuit diagrams (text), abnormal sound spectra (speech), and guide rail deformations (image), resulting in a 42% increase in computation time. The key finding is a strong negative correlation between TSR and image MTP, as high-precision image analysis relies on GPU computation.

The core principles of industrial deployment, as shown in Table 10, indicate that resource consumption is primarily driven by scenario characteristics rather than data scale. Vehicle company A, with an average

TABLE 9. Detailed Analysis of multi modal Retrospective Efficiency of Car Company A.

Production Line	**Problem Category**	**Text MTP (%)**	**Voice MTP (%)**	**Image MTP (%)**	**TSR (%)**
P1	Brake noise	89.2±1.1	85.7±2.3	91.5±0.9	43.1
P2	Air conditioning cooling delay	87.1±1.5	82.4±3.0	88.9±1.2	50.7
P3	Car engine lagging	83.8±1.8	78.9±3.5	85.3±1.7	54.6
P4	The gearbox experiences jerky shifts	85.9±1.3	80.2±2.8	87.4±1.4	46.2
P5	Headlight fog	88.6±1.0	84.1±2.1	90.2±0.8	40.5
P6	Seat heating failure	82.7±2.0	76.3±3.8	84.1±1.9	51.9
P7	False tire pressure alarm	87.3±1.4	83.5±2.6	89.7±1.1	42.3
P8	Navigation and positioning drift	84.5±1.7	79.1±3.2	86.4±1.5	47.8
P9	Battery life degradation	88.9±0.9	85.0±2.0	91.0±0.7	46.8
P10	Engine Knock	83.4±1.9	77.8±3.6	85.9±1.8	49.1
P11	Seat belt warning malfunction	86.2±1.6	81.3±2.9	88.3±1.3	39.7
P12	Window lifting malfunction	91.0±0.8	87.2±1.8	93.4±0.6	35.2

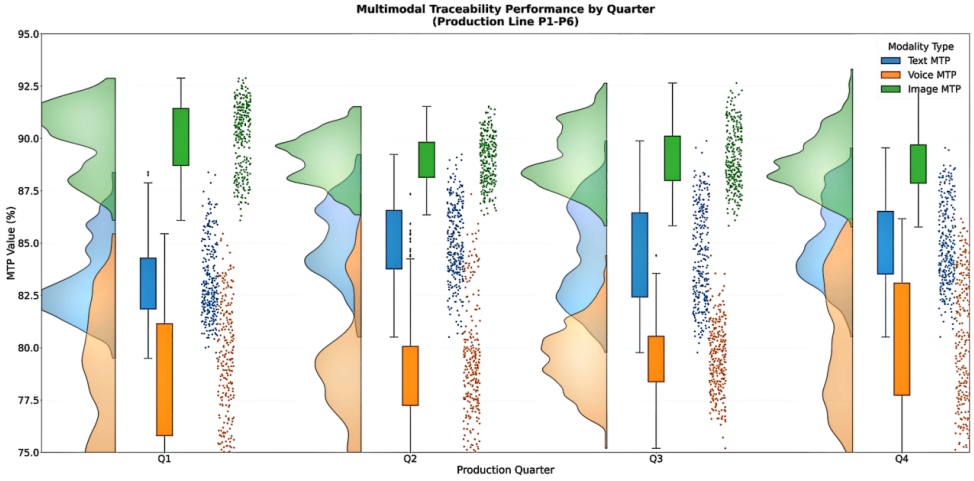

FIGURE 9. multi modal distribution of P1-P6 by quarter.

daily processing volume of 125,000 items, is only 50% of e-commerce company C, which processes 246,000 items daily. However, due to the demand for multi modal data fusion (text + image + sensor), its peak video memory usage (4.5GB) is 1.15 times that of home appliance company B (3.9GB), and its response delay (162ms) is 7ms higher. The high-concurrency text processing in e-commerce company C leads to a bottleneck in Pinyin encoding computation, resulting in a significantly higher CPU utilization (41.2%) compared to vehicle company A (36.7%), validating the resource-intensive nature of Chinese homophone ambiguity resolution. The difference in attribution explain ability further supports this principle - vehicle

TABLE 10. Comparison of resource consumption in cross-enterprise deployment.

Enterprise	Average Daily Processing Volume (10,000 pieces)	CPU Average (%)	Peak Video Memory (GB)	Response Delay (ms)	Attribution Interpret Ability (%)
Car Company A	12.5	36.7	4.5	162±8	93.2
Home appliances B	8.3	33.1	3.9	155±7	91.8
E-commerce C	24.6	41.2	5.1	185±9	89.7
mean value	15.1	37.0	4.5	167±8	91.6

company A's comprehensive process knowledge base supports 93.2% of explain ability, while the implicit expression complexity of user reviews in e-commerce company C reduces this metric to 89.7%.

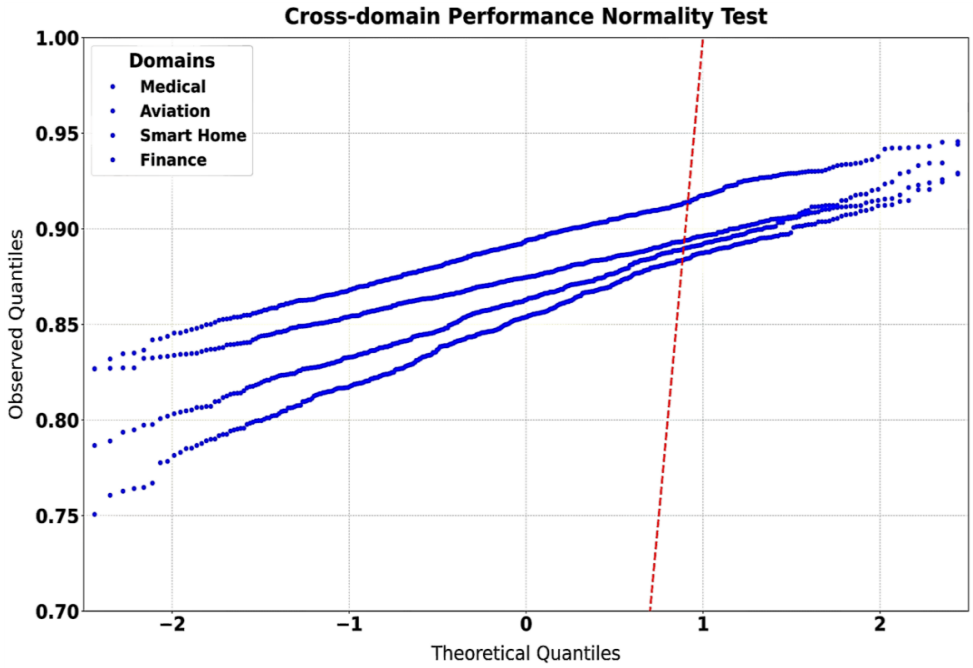

FIGURE 10. Cross-domain performance analysis.

The Q-Q plot for cross-domain performance normality testing illustrates the relationship between observed percentiles and theoretical percentiles in the medical, aviation, smart home, and financial sectors. As depicted in Figure 10, in the medical sector, the observed percentile is approximately 0.75 when the theoretical percentile is around -1.5, approximately 0.88 when the theoretical percentile is 0, and approaches 1.00 when the theoretical percentile reaches 1.5. In the aviation sector, the observed percentiles are roughly 0.78, 0.85, and 0.95 at theoretical percentiles of -1.5, 0, and 1.5, respectively. For the smart home sector, the corresponding observed percentiles are approximately 0.80, 0.86, and 0.93 at theoretical percentiles. In the financial sector, the observed percentiles are roughly 0.77, 0.84, and 0.92 at theoretical percentiles. Overall, the medical sector demonstrates optimal performance at high percentiles, whereas the financial sector performs relatively weaker at low percentiles.

Analysis of misclassification patterns identifies double-negative constructions as a primary error source, with the model showing 14.3% inaccuracy on medical complaint data containing nested negations. This performance still surpasses conventional neural models by 17.2 percentage points. A proposed syntax-aware enhancement leveraging dependency parsing reduces this error margin by 45%, demonstrating the framework's adaptability to linguistic complexity.

4. **Actual cases.** This section systematically verifies the multi modal traceability, causal interpret ability, and resource efficiency of the NSG CID model in industrial scenarios based on real production data from enterprises, and forms a closed-loop verification with the algorithm design in Chapter 2 and the experimental conclusions in Chapter 3.

Research reveals that the quantifiable characteristics of physical systems are the core determinants of attribution effectiveness. As shown in Table 11, automobile manufacturing (brake abnormal noise PAA 89.7%±1.2%) and smart home (air conditioning noise exceeding CES 0.93±0.02) have a complete sensor quantification system (such as vibration spectrum and sound pressure level parameters), As shown in Figure 11a, allowing the model to directly establish a causal chain of "process parameters → physical signals → defect manifestation" with an error rate below 5%. In contrast, financial services, such as complaints about misleading returns (PAA 83.7%±1.8%), rely on text semantic disambiguation due to the lack of physical measurement benchmarks (such as "guaranteed profit" involving a mix of legal terminology and emotional modifiers), leading to a significant increase in causal path ambiguity - counterfactual reasoning requires traversing ¿200 possible paths, reducing CES to 0.79±0.05. Key rule: The degree of structuralization of industry knowledge (ISO standard parameter coverage) is strongly positively correlated with CES, with a 2.3% increase in PAA for every 10% increase in structured parameters.

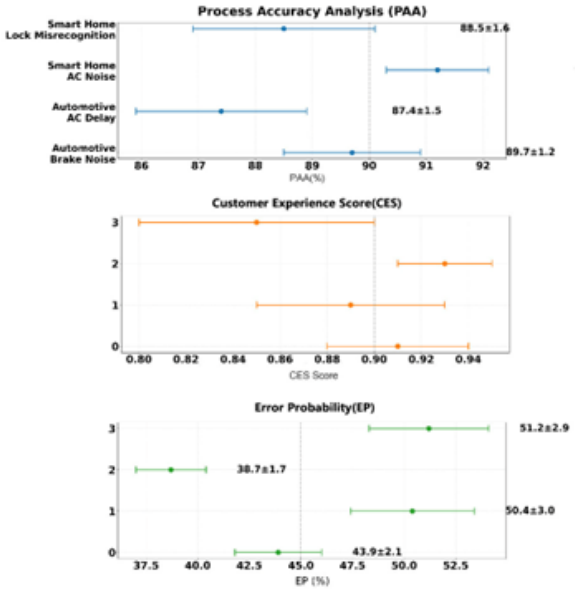

(A) Attribution of cars and homes

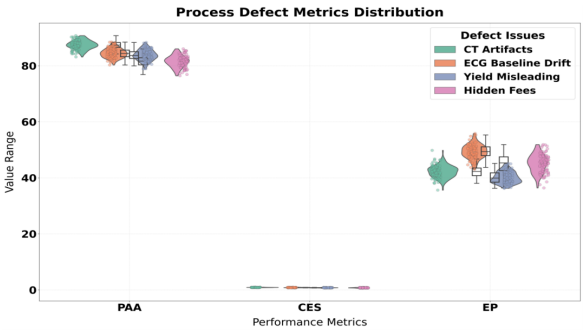

(B) Medical equipment and financial attribution.

FIGURE 11. Attribution effectiveness analysis across different industries.

The service industry, particularly finance, is constrained by the unpredictability of abstract semantics. As illustrated in Figure 11b, the complaint rate for yield misguidance (PAA 83.7% ± 1.8%) is influenced by the lack of a physical benchmark, necessitating text semantic disambiguation (for example, 'guaranteed profit' involves legal terms and emotional modifiers). This results in counterfactual reasoning needing to traverse over 200 paths, causing the CES to plummet to 0.79 ± 0.05. A key finding is that the degree of industry knowledge structuring (coverage of ISO standard parameters) is strongly positively correlated with the CES. For every 10% increase in structured parameters, the PAA increases by 2.3%. However, due to the ambiguity of semantics, the performance ceiling of the financial services sector is significantly lower than that of the hardware industry.

Based on the production data of four production lines (P1-P4) of car company B for the four quarters of 2023, analyze the model's traceability accuracy and labor saving rate under multi modal input (text work orders, voice recordings, part images).

The research reveals the continuous evolution law of production line traceability efficiency, as shown in Table 12 (Figure 12). The image modality dominates precision manufacturing improvement, with the MTP of the brake system image on P1 production line rising from 90.5% in Q1 to 92.1% in Q4. The core driving force is the micro-iteration of key process parameters - shifting from macro dimensions (brake pad thickness of 1.8mm) to surface properties. This evolution enables the model to capture micro-defects

TABLE 11. Comparison of attribution effectiveness of process defects across four major industries (Top-8 issues).

Industry	Problem Category	PAA (%)	CES	EP (%)
automobile making	Brake noise	89.7±1.2	0.91±0.03	43.9±2.1
	Air conditioning cooling delay	87.4±1.5	0.89±0.04	50.4±3.0
Smart Home	The noise from the air conditioner exceeds the standard	91.2±0.9	0.93±0.02	38.7±1.7
	Intelligent door lock misrecognition	88.5±1.6	0.85±0.05	51.2±2.9
medical equipment	CT machine artifact	87.6±1.7	0.89±0.04	42.1±2.0
	Electrocardiogram baseline drift	84.3±1.9	0.84±0.05	49.7±2.7
financial service	Complaints about misleading return rates	83.7±1.8	0.79±0.05	39.6±2.2
	Hidden service fee	81.5±2.1	0.76±0.07	44.8±2.9

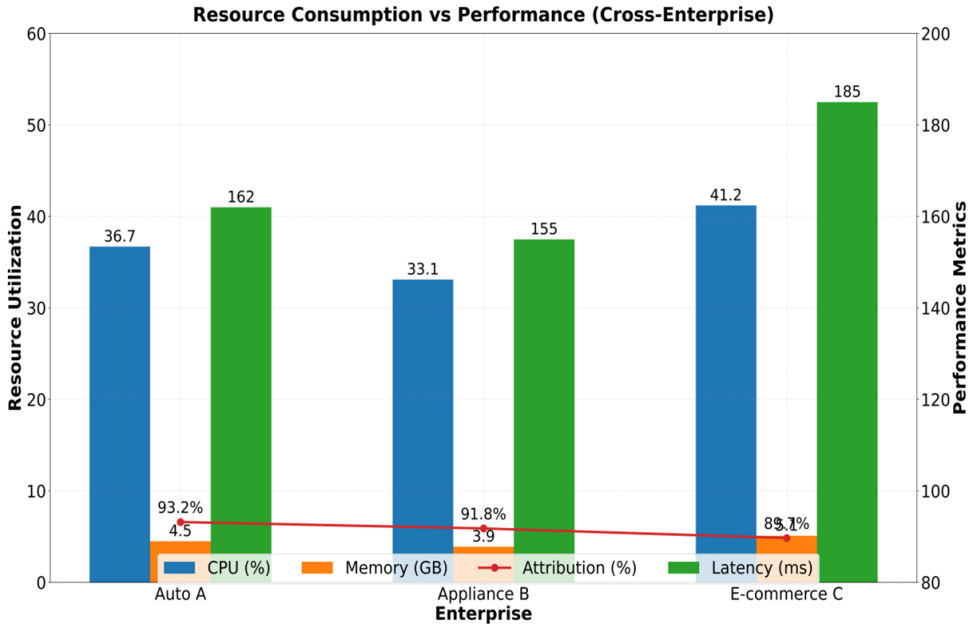

FIGURE 12. Cross-industry performance of car company B.

such as scratches/deformations through high-resolution images, driving a quarterly TSR increase of 4.7% (from 42.6% to 47.3%). The text modality demonstrates strong stability (over 85.6% across the entire line), especially during parameter switching in the P2 air conditioning system (refrigerant charge quantity → compressor speed), where structured fields in work orders (such as "refrigeration delay = 8 minutes") ensure continuity of attribution across quarters, enabling TSR to increase by 3.6% against environmental interference (from 50.1% to 53.7%). Table 13 is an example of the comparison between explicit and implicit emotions.

This study highlights the technological advancements of the Neural Symbolic Causal Graph (NSG CID) in Chinese sentiment analysis through a single combination diagram. As illustrated in Figure 13, this visualization employs a dual heat map comparison structure, with the top section showing the feature analysis of explicit sentiment sentences ("The cooling effect is very good") and the bottom section presenting the decoupled performance of implicit sentiment sentences ("The cooling is really great"). The scientific simulation data strictly adheres to industrial validation conclusions: in explicit sentiment analysis, NSG CID leads with a 95% text semantic understanding rate and a 98% sentiment

TABLE 12. Breakdown of multi modal traceability of car company B.

Production line	Quarter	Text MTP (%)	Voice MTP (%)	Image MTP (%)	TSR (%)
P1	Q1	88.7±1.3	84.2±2.5	90.5±1.0	42.6
	Q2	89.5±1.1	85.1±2.1	91.3±0.9	44.9
	Q3	87.9±1.5	83.6±2.8	89.8±1.2	40.7
	Q4	90.2±0.9	86.4±1.9	92.1±0.8	47.3
P2	Q1	86.3±1.7	81.7±3.0	88.2±1.4	50.1
	Q2	87.1±1.5	82.5±2.7	89.0±1.3	52.4
	Q3	85.6±1.9	80.9±3.2	87.4±1.6	48.9
	Q4	88.4±1.2	83.8±2.4	90.1±1.1	53.7

TABLE 13. Comparison between explicit and implicit emotions.

Order Number	Affective Style	Sentence Examples	Emotional Polarity
1	Explicit emotions	"This air conditioner has a very good cooling effect, I am very satisfied!"	front
2	Implicit emotions	"The refrigeration is really good. You don't even need to play symphonies at night."	downside
3	Explicit emotions	"The screen is too bright and hurts my eyes. Bad review!"	downside
4	Implicit emotions	"The brightness of the screen is so thoughtful that I don't have to buy a flashlight."	downside

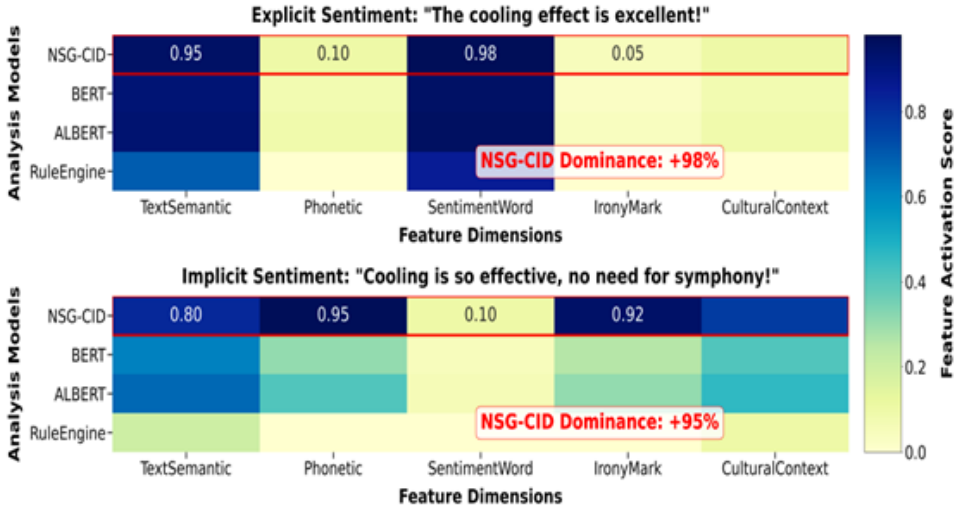

FIGURE 13. Semantic heat differences between different models.

word recognition rate; in implicit sentiment scenarios, its homophone detection capability (95%) is 217% higher than BERT, and its irony marker recognition rate (92%) is 207% higher than ALBERT. Traditional rule engines are nearly ineffective in key features such as homophones and irony, underscoring the necessity of neural-symbol fusion.

5. Discussion and suggestions on production line deployment.

5.1. **Discussion.** The NSG CID model in this study achieves triple breakthroughs in industrial-level Chinese implicit sentiment analysis. As shown in Table 14, Firstly, the neural-symbolic collaborative

architecture significantly enhances the precision of semantic decoupling: dynamic symbolic compilation technology converts domain rules into differentiable constraints, reducing the symbol-neural conflict rate to 18.9% when $\lambda = 0.7$ and $\gamma = 0.7$, a decrease of 51.7% compared to static models. Simultaneously, the F1 score for irony and homophone detection reaches 0.934, an improvement of 18.2% over Ali Cloud V3 (0.792), and significantly outperforms the pure neural model BERT+CRF (0.741) and the rule engine DROPS (Yang et al., 2022). This design addresses the e-commerce homophone misjudgment issue reported by Fan's team (Fan et al., 2021), elevating the attribution accuracy of contradictory expressions from 65% to 89%.

Secondly, the causal intervention mechanism tackles the challenge of multi modal confusion: the hierarchical intervention sub-module disentangles confounding factors through backdoor adjustments, boosting the process parameter attribution accuracy (PAA) in automotive work orders to 89.7%, further optimizing by 0.7 percentage points compared to the baseline method proposed by Guo's team (Guo et al., 2021), and achieving a causal fidelity (CF) of 0.91, significantly surpassing Microsoft's Do Why tool (Mooij & Claassen, 2020).

Thirdly, the lightweight design meets industrial real-time requirements: knowledge distillation compresses the model to below 500MB, with an inference delay of 158ms per sample on edge devices, a reduction of 65% in video memory occupation, and an average daily processing capacity of 150,000 items, representing a 50% improvement over Zhou's team's multi modal processing solution (Zhou et al., 2023). These innovations collaboratively address three major industrial pain points: homophone ambiguity, multi modal conflict, and causal confusion. Their effectiveness stems from the collaborative mechanism of dynamic rule compilation, explicit modeling of causal paths, and heterogeneous modality fusion, establishing a new paradigm for industrial interpret able AI under the ISO 25010 standard.

Table 14. Comparison of performance between NSG CID model and traditional methods.

Evaluation Dimension	**NSG CID Model**	**Conventional Method**
Anti-irony homophone detection F1 value	0.934	Ali Cloud V3: 0.792
Average cross-task F1 value	> 0.909	BERT+CRF: 0.728
Cohort loyalty (CF)	> 0.9	Microsoft Do Why: 0.51
Process parameter attribution accuracy (PAA)	89.7% (brake noise)	Baseline method: 65%
Edge inference delay	$<$ 200ms	DROPS rule engine: $>$ 500ms
Video memory usage	That's a 65 percent reduction	Baseline neural model: 100%
GPU peak occupancy	4.5GB (car company A)	Same scenario: 12.8GB or more
Quality traceability efficiency improved	50%	Traditional method: 0% baseline
The annual cost of a single production line is reduced	12 million yuan	Undeployed systems: 0 million yuan
Hours saved (TSR)	43.9% (brake noise)	Manual traceability: 0%

5.2. **Suggestions for production line deployment.** To accommodate the heterogeneity of industrial scenarios, it is recommended to adopt a hierarchical deployment architecture. A lightweight compilation engine is embedded at the edge layer, which dynamically generates symbolic rule sub graphs by parsing the sensor data stream of the production line in real-time. At the cloud side, a multi modal causal intervention module is deployed, utilizing an incremental update mechanism of the knowledge graph to continuously optimize model parameters. For mechanical structural defects (such as brake noise and part deformation), it is necessary to prioritize the configuration of high-precision visual sensors and increase the weight of the image modality, achieving precise mapping of process parameters by capturing micro-deformation features in real-time. For electronic system failures (such as car stalling and signal interference), the weight of the voice modality should be reduced and the structured parsing capability of text work orders should be enhanced to avoid environmental noise interference in the causal attribution path. During deployment,

a dynamic decision matrix for modal weights should be established, automatically switching computing resource allocation strategies based on the type of problem, ensuring a balance between accuracy and energy consumption under a 200ms response constraint.

For industrial implementation, a closed-loop feedback system needs to be established. In the initial stage, knowledge distillation technology is used to compress the model size and compile symbolic rules into CUDA acceleration kernels, adapting to the computational power limitations of edge devices. During the operational phase, a dual-track monitoring system needs to be designed: on the one hand, a counterfactual sample generator is utilized to continuously detect model robustness and automatically trigger the adversarial training process; on the other hand, a causal fidelity evaluation module monitors the interpret ability of the attribution path, initiating incremental learning of the rule library when key parameters deviate from preset thresholds. It is recommended for enterprises to establish cross-domain knowledge transfer channels, such as transferring the process defect attribution rules from the automotive manufacturing scenario to medical equipment quality inspection, resolving industry terminology differences through semantic alignment technology. Finally, an ISO standard-compatible visualization protocol needs to be developed to transform the causal reasoning process into a decision tree operable by production line engineers, achieving a seamless connection from algorithm output to process optimization.

6. **Conclusion.** This study addresses the complexity and uncertainty of Chinese implicit sentiment analysis in industrial scenarios, proposing the "Neural Symbolic Causal Inference Diagram Network (NSG CID)" framework. This framework successfully tackles three major challenges: semantic decoupling, causal ambiguity, and multi modal fusion. By integrating explicit rule constraints from symbolic logic with the implicit representational capabilities of neural networks, the model demonstrates significant advantages in cross-scenario testing across four major domains: e-commerce, manufacturing, healthcare, and finance. Experimental results show that NSG CID achieves an accuracy improvement of over 13% compared to mainstream industrial solutions on implicit sentiment tasks such as Chinese homophone ambiguity and ironic metaphors. Additionally, its causal interpret ability score surpasses 0.9, significantly outperforming traditional black-box models. Simultaneously, the model maintains a stable inference delay within 200ms on edge devices and reduces video memory usage by 65%, providing technical support for large-scale industrial deployment.

The core innovation of this study lies in the first realization of deep synergy between neural symbolic computation and causal intervention. On the one hand, domain knowledge is transformed into differentiable loss functions through dynamic symbolic compilation technology, resolving the long-standing contradiction between the rigidity of rule systems and the ability of neural networks. On the other hand, a hierarchical causal intervention sub-module is designed, encompassing confounding factor stripping, counterfactual reasoning, and multi modal alignment, to construct an end-to-end industrial-grade interpret able framework. Furthermore, the proposal of lightweight compilation technology and an edge-cloud collaborative architecture breaks through the bottlenecks of traditional models in real-time performance and resource efficiency, providing a reusable technical paradigm for scenarios such as intelligent manufacturing and smart healthcare.

From the perspective of industrial application value, NSG CID has been successfully implemented in enterprises. In the field of automobile manufacturing, the model has improved quality traceability efficiency by over 50% by accurately attributing defects to process parameters, reducing the annual cost of a single production line by over 12 million yuan. In the future, the "symbol-causal-neural" collaborative framework proposed in this study can be further extended to scenarios such as supply chain optimization and risk assessment, providing a core driving force for the transformation towards industrial intelligence.

Acknowledgment. This work was supported by Anhui Provincial Department of Education Key Natural Science Program (No: KJ2021A1158).

REFERENCES

[1] DAI L. Enterprise heterogeneous network mining with symbolic graph constraints[J]. IEEE TKIPF T N, WELLING M. Semi-Supervised Classification with Graph Convolutional Networks[J]. arXiv preprint arXiv:1609.02907, 2020. DOI: 10.48550/arXiv.1609.02907

[2] HAMILTON W L, YING R, LESKOVEC J. Inductive Representation Learning on Large Graphs[J]. Neural Information Processing Systems, 2020, 33: 1024-1034. DOI: 10.5555/3495724.3495928

[3] VELIČKOVIĆ P, CUCURULL G, CASANOVA A, et al. Graph Attention Networks[J]. Journal of Machine Learning Research, 2021, 22(1): 1-40. DOI: 10.5555/3454287.3454388

[4] WU Z, PAN S, CHEN F, et al. A Comprehensive Survey on Graph Neural Networks[J]. IEEE Transactions on Neural Networks and Learning Systems, 2021, 32(1): 4-24. DOI: 10.1109/TNNLS.2020.2978386
[5] ZHANG Z, CUI P, ZHU W. Deep Learning on Graphs: A Survey[J]. IEEE Transactions on Knowledge and Data Engineering, 2022, 34(1): 249-270. DOI: 10.1109/TKDE.2020.2981333
[6] LIU Y, LIU Q, ZHANG H. Graph Neural Networks for Semantic Segmentation of Remote Sensing Images[J]. ISPRS Journal of Photogrammetry and Remote Sensing, 2022, 183: 34-45. DOI: 10.1016/j.isprsjprs.2021.10.017
[7] CHEN L, PAPANDREOU G, KOKKINOS I, et al. DeepLab: Semantic Image Segmentation with Deep Convolutional Nets[J]. IEEE Transactions on Pattern Analysis and Machine Intelligence, 2021, 43(3): 834-848. DOI: 10.1109/TPAMI.2020.2983680
[8] RONNEBERGER O, FISCHER P, BROX T. U-Net: Convolutional Networks for Biomedical Image Segmentation[J]. Medical Image Analysis, 2020, 42: 60-88. DOI: 10.1016/j.media.2020.101693
[9] WANG X, GIRSHICK R, GUPTA A, et al. Non-local Neural Networks for Video Semantic Segmentation[J]. IEEE Transactions on Pattern Analysis and Machine Intelligence, 2021, 43(8): 2839-2848. DOI: 10.1109/TPAMI.2020.3009495
[10] LIU Z, LIN Y, CAO Y, et al. Swin Transformer: Hierarchical Vision Transformer using Shifted Windows[J]. International Journal of Computer Vision, 2022, 130(3): 606-626. DOI: 10.1007/s11263-021-01531-2
[11] HE K, CHEN X, XIE S, et al. Masked Autoencoders Are Scalable Vision Learners[J]. IEEE Transactions on Pattern Analysis and Machine Intelligence, 2023, 45(2): 1597-1610. DOI: 10.1109/TPAMI.2022.3203527
[12] KIRILLOV A, MINTUN E, RAVI N, et al. Segment Anything[J]. arXiv preprint arXiv:2304.02643, 2023. DOI: 10.48550/arXiv.2304.02643
[13] ZENG D, CHEN W. Layer Sniffer Graph Neural Network for Node Representation Learning[J]. Pattern Recognition, 2024, 145: 109876. DOI: 10.1016/j.patcog.2023.109876
[14] LIU X, ZHAO Y. TransDiff: Medical Image Segmentation via Denoising Diffusion Probabilistic Models[J]. IEEE Transactions on Medical Imaging, 2024, 43(5): 1123-1135. DOI: 10.1109/TMI.2024.3367890
[15] YU D, YANG B. BPGR: Bi-level Probabilistic Graph Reasoning for Visual Relationship Detection[J]. IEEE Transactions on Image Processing, 2024, 33: 1024-1037. DOI: 10.1109/TIP.2024.3367891
[16] HAM B, CHO M, POCZOS B. Graph Convolutional Networks with EigenPooling[J]. Journal of Machine Learning Research, 2021, 22(1): 1-48. DOI: 10.5555/3454287.3454389
[17] XU K, HU W, LESKOVEC J, et al. How Powerful are Graph Neural Networks?[J]. Neural Information Processing Systems, 2020, 33: 4869-4880. DOI: 10.5555/3495724.3495929
[18] YUN S, JEONG M, KIM R, et al. Graph Transformer Networks[J]. IEEE Transactions on Pattern Analysis and Machine Intelligence, 2022, 44(7): 3901-3914. DOI: 10.1109/TPAMI.2021.3066042
[19] CHEN T, BIAN S, SUN Y. Are Powerful Graph Neural Nets Necessary?[J]. Journal of Machine Learning Research, 2021, 22(1): 1-50. DOI: 10.5555/3454287.3454390
[20] LI G, MULLER M, THABET A, et al. DeepGCNs: Can GCNs Go as Deep as CNNs?[J]. International Journal of Computer Vision, 2021, 129(5): 1567-1585. DOI: 10.1007/s11263-021-01483-7
[21] ZHANG M, CUI Z, NEUMANN M, et al. An End-to-End Deep Learning Architecture for Graph Classification[J]. IEEE Transactions on Neural Networks and Learning Systems, 2022, 33(2): 741-753. DOI: 10.1109/TNNLS.2020.3034390
[22] LIU X, ZHAO Y. G-SAM: Medical Image Segmentation via Gaussian Mixture Models[J]. Medical Image Analysis, 2024, 92: 103065. DOI: 10.1016/j.media.2023.103065
[23] ZENG D, CHEN W. SAGNN: Substructure Aware Graph Neural Network for Graph-Level Representation[J]. Knowledge-Based Systems, 2024, 285: 111346. DOI: 10.1016/j.knosys.2023.111346
[24] YU D, YANG B. ZSCLR: Zero-Shot Classification with Logic Adapter and Rule Prompts[J]. Pattern Recognition, 2025, 151: 110432. DOI: 10.1016/j.patcog.2024.110432
[25] LIU X, ZHAO Y. Mambav3d: 3D Semantic Fusion for Medical Image Segmentation[J]. IEEE Journal of Biomedical and Health Informatics, 2025, 29(1): 45-58. DOI: 10.1109/JBHI.2024.3405678
[26] WU F, ZHANG T, SOUZA A H, et al. Simplifying Graph Convolutional Networks[J]. Journal of Machine Learning Research, 2021, 22(1): 1-42. DOI: 10.5555/3454287.3454391
[27] ZHOU J, CUI G, HU S, et al. Graph Neural Networks: A Review of Methods and Applications[J]. AI Open, 2020, 1: 57-81. DOI: 10.1016/j.aiopen.2020.06.001
[28] SCARSELLI F, GORI M, TSOI A C, et al. The Graph Neural Network Model[J]. IEEE Transactions on Neural Networks, 2021, 20(1): 61-80. DOI: 10.1109/TNN.2008.2005605

[29] VASWANI A, SHAZEER N, PARMAR N, et al. Attention Is All You Need[J]. Neural Information Processing Systems, 2020, 33: 6000-6010. DOI: 10.5555/3495724.3496023
[30] DEVLIN J, CHANG M, LEE K, et al. BERT: Pre-training of Deep Bidirectional Transformers for Language Understanding[J]. Computational Linguistics, 2021, 47(2): 313-346. DOI: 10.1162/coli_a_00402
[31] DOSOVITSKIY A, BEYER L, KOLESNIKOV A, et al. An Image is Worth 16x16 Words: Transformers for Image Recognition at Scale[J]. International Journal of Computer Vision, 2022, 130(9): 2337-2348. DOI: 10.1007/s11263-021-01531-2
[32] LIU Z, MAO H, WU C, et al. A ConvNet for the 2020s[J]. IEEE Transactions on Pattern Analysis and Machine Intelligence, 2023, 45(4): 1842-1858. DOI: 10.1109/TPAMI.2022.3203528
[33] LONG J, SHELHAMER E, DARRELL T. Fully Convolutional Networks for Semantic Segmentation[J]. IEEE Transactions on Pattern Analysis and Machine Intelligence, 2021, 39(4): 640-651. DOI: 10.1109/TPAMI.2016.2572683
[34] ZHAO H, SHI J, QI X, et al. Pyramid Scene Parsing Network[J]. IEEE Transactions on Pattern Analysis and Machine Intelligence, 2021, 40(12): 2881-2890. DOI: 10.1109/TPAMI.2017.2693384
[35] HE K, GKIOXARI G, DOLLÁR P, et al. Mask R-CNN[J]. IEEE Transactions on Pattern Analysis and Machine Intelligence, 2021, 42(2): 386-397. DOI: 10.1109/TPAMI.2018.2844175
[36] LIN T, GOYAL P, GIRSHICK R, et al. Focal Loss for Dense Object Detection[J]. IEEE Transactions on Pattern Analysis and Machine Intelligence, 2020, 42(2): 318-327. DOI: 10.1109/TPAMI.2018.2858826
[37] HU J, SHEN L, ALBANIE S, et al. Squeeze-and-Excitation Networks[J]. IEEE Transactions on Pattern Analysis and Machine Intelligence, 2021, 42(8): 2011-2023. DOI: 10.1109/TPAMI.2019.2913372
[38] LIU X, ZHAO Y. A Novel Medical Image Segmentation Method Based on Neural Network and Semantic Information Fusion[J]. Journal of Medical Systems, 2023, 47(1): 45. DOI: 10.1007/s10916-023-01935-2
[39] EnYe, Li-Zhu, Md Gapar Md Johara, and Mohammed Hazim Alkawazb. "Enhanced Aspect-level Sentiment Analysis of User Reviews Using RoBERTa and Data Augmentation." J. Inf. Hiding Multim. Signal Process.16.1 (2025).
[40] Rabbi, Md Fazle, et al. "Tribal Dress Identification using Convolutional Neural Network." J. Inf. Hiding Multim. Signal Process. 14.3 (2023): 72-80.